Thickness dependence of spin wave excitations in an artificial square spin ice-like geometry

Y. Li,[1] G. Gubbiotti,[2] F. Casoli,[3] S. A. Morley,[4] F. J. T. Gonçalves,[1] M. C. Rosamond,[5] E. H. Linfield,[5] C. H. Marrows,[4] S. McVitie,[1] and R. L. Stamps[1]
[1]*School of Physics and Astronomy, University of Glasgow, Glasgow G12 8QQ, United Kingdom*
[2]*Istituto Officina dei Materiali del Consiglio Nazionale delle Ricerche, Sede Secondaria di Perugia, c/o Dipartimento di Fisica e Geologia, Via A. Pascoli, I-06123 Perugia, Italy*
[3]*IMEM-CNR, I-43124 Parma, Italy*
[4]*School of Physics and Astronomy, University of Leeds, Leeds LS2 9JT, United Kingdom*
[5]*School of Electronic and Electrical Engineering, University of Leeds, Leeds LS2 9JT, United Kingdom*

(Received 14 September 2016; accepted 25 February 2017; published online 10 March 2017)

We present a comparative study of the spin wave properties in two magnetic films patterned into an artificial square spin ice-like geometry. The array elements are rectangular islands with the same lateral dimensions but with different thicknesses: 10 nm and 30 nm. Using Brillouin light scattering, the frequencies of spin wave excitations were measured as a function of the magnetic field going from positive to negative saturation. We find substantial changes with thickness to spin wave mode frequencies and the number of detected modes. Frequencies of spin waves localized at element edges are observed to evolve non-monotonically with magnetic fields and soften at critical fields. These critical fields enable us to extract information of the magnetization reversal of individual islands within the array. Finally, we discuss the effects of separation between islands and examine the possibilities for dynamic coupling through the overlap of collective edge modes.
[http://dx.doi.org/10.1063/1.4978315]

I. INTRODUCTION

Patterning of ferromagnetic films into closely spaced, single domain islands can be used to create arrays of mesoscopic magnets often termed artificial spin ice (ASI).[1] Square ASI is one of the first and best studied ice geometries.[2–5] The magnetic elements in these structures are usually ferromagnetically elongated islands with a large uniaxial shape anisotropy whose behaviour can be approximated as Ising spins. These magnetic elements interact via static magnetic stray dipolar fields.[6,7] In closely square spaced arrays, the dipolar inter-element interactions can be engineered to favour antiferromagnetic ordering.[8] It has been shown recently that the offset of the two sublattices can recover a truly water ice-like geometrical frustration in the square ice geometry which no longer favours antiferromagnetic order.[9]

The spin wave (SW) properties of rectangular magnetic islands have been well investigated individually and in a variety of array geometries.[10–13] Many types of SW eigenmodes have been identified in the GHz frequency range whose character is determined by the dynamic dipolar interaction. Some works have recently appeared which measured the ferromagnetic resonance (FMR) and SWs in magnetic-element arrays with a number of ASI geometries, such as square, penrose, and kagome, etc.[14–22] The work of Yahagi *et al.*[21] reveals two SW eigenmodes responding to the two magnetization orientations of two sub-lattices of an elliptic-disk array which align collinear or orthogonal to the magnetic field. By way of contrast, we show that a rich spectrum of confined SW eigenmodes can be detected with Brillouin light scattering (BLS). These eigenmodes can be used to identify details of the magnetization processes occurring during magnetic reversal and hysteresis that cannot be resolved using ferromagnetic resonance (FMR) or magnetometry.

In this paper, we present measurements of SW frequencies on square ASI-like structure in the GHz range obtained using BLS. SWs in magnetic element geometries possess a stationary character[23] and the dipolar stray fields associated with eigenmodes localized to the element edges extend outside elements,[12] decaying with distance into the region between elements.[24] We report a comparative study of hysteresis loops and SW excitations obtained from two different ASI-like arrays of 10 nm and 30 nm thicknesses. It is worthy to note that a part of the results of 10 nm thick ASI-like array can be found in the Li *et al.* paper.[22] Emphasis has been given to the presence of soft magnetic eigenmodes which accompany the magnetization reorientation and switching of islands.[25,26] The case of the easy axis aligned parallel and orthogonal to the applied field direction is presented here. As a study of possible edge mode interaction, we also examine numerically the dependence of SWs on the separation between islands.

II. SAMPLE PROPERTIES AND RESULTS

Two magnetic island arrays were fashioned into square ASI-like geometry from 10 nm and 30 nm thick $Ni_{80}Fe_{20}$ films. Patterning was done on an oxidised-silicon substrate using electron-beam lithography. The lateral dimension of each island is $240 \times 80\,nm^2$ and the centre-to-centre

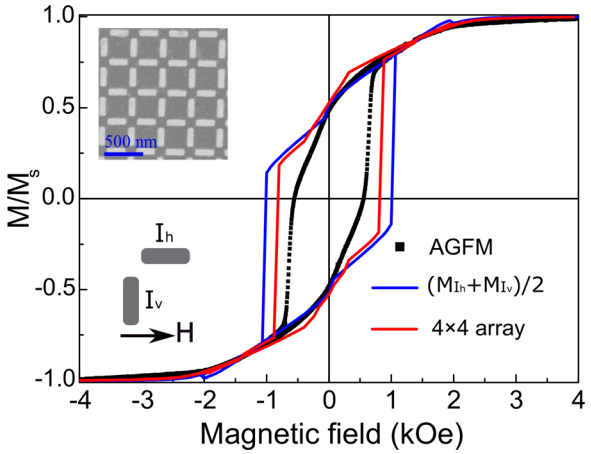

FIG. 1. AGFM (black square) and simulated (lines) hysteresis loops of the 30 nm thick ASI-like array with the magnetic field H applied parallel to one sublattice of ASI-like islands. Blue line represents the mean value of the isolated I_h and I_v island loops, which are depicted at the bottom left, and red line presents the hysteresis loop of the 4×4 units array. Inset at the top left is SEM images of the ASI-like array.

separation between the second nearest islands was chosen to be 450 nm. Correspondingly, the corner-to-corner distance, d, between the first nearest neighbouring islands is around 92 nm. Scanning electron micrograph (SEM) of the measured ASI-like specimen is shown in the inset of Fig. 1.

Hysteresis loops were measured using alternating gradient force magnetometer (AGFM) with magnetic field applied parallel to one of the elements' easy axes, and the applied field was swept between +4 kOe and −4 kOe. The measured AGFM hysteresis loops with the magnetic field applied parallel to the long axis of one sub-lattice of the elements are shown in Fig. 1 by the black squares. Results for the 30 nm thick elements in Fig. 1 and for the 10 nm thick elements are shown in the published paper.[22] As a bulk technique, AGFM probes the magnetic moment of the entire array therefore the derived information is a superposition of the magnetization components associated with different element orientations with respect to the applied field. There is a step which is visible at the zero field for the thin elements[22] that is, however, not visible for the thicker elements in Fig. 1. In addition, Table I shows that the measured coercive field of the 10 nm thick array (≈0.365 kOe) is smaller than that of the 30 nm thick one (≈0.553 kOe).

Micromagnetic simulations have been performed by MuMax3 GPU-based micromagnetic simulator[27] using the following parameter values. The saturation magnetization M_s and exchange stiffness constant A of permalloy ($Ni_{80}Fe_{20}$) material were taken as 800 kA/m and 10×10^{-12} J/m, respectively.[28] A grid with 10 nm (or 30 nm) thickness and around 2.4 nm × 2.4 nm lateral size of cell was used which is less than the exchange length (∼5 nm).[29] Simulations were performed assuming infinite spacing between elements so that hysteresis is an average of magnetization from elements aligned parallel and perpendicular to the applied field which are presented in Fig. 1 by blue lines. Although this approximation cannot well describe the hysteresis measured for the 30 nm thick element (see Fig. 1), it matches better with that of the 10 nm film array.[22] Likewise, Table I illustrates that the coercivity difference of 10 nm thickness between experimental value and simulated average is three times less than that of the 30 nm thick sample. This suggests a possible stronger interelement coupling for the thicker array. To test this, simulations for a 4×4 units array, in which one unit consists of four elements, were made and results are displayed by red lines in Fig. 1. A better agreement of the coercivity of 30 nm thick element between simulation and experiment is visible if we take the errors into account. However, the experimental curve of the thicker array appears smoother than those of the simulated loops, which show two evident and sharp steps in the vicinity of zero and coercive field. The reason may be the contribution of the edge/volume disorders,[30] which results in a distribution of switching fields which means an initial switch of an island's magnetization can happen at a field lower than the average coercivity but then be propagated through the array due to interactions.[6,31] This disorder is not accounted for in the simulations where the isolated I_v (I_h) island or all vertical (horizontal) islands of the array reverse simultaneously which is responsible for the sharp step near the zero field (coercive field).

An estimation of the static field interaction was made using the micromagnetic simulation. The energy difference $\Delta E = E_- - E_+$ of the central element shown in Fig. 2(a) was calculated for two orientations: one aligned parallel to the static field produced by the neighbours (E_+), and one for the reversed orientation (E_-). The corresponding static field magnitude is $H_s = -\Delta E/(M_s V)$, where V is the volume of island. Note that there are sixteen possibilities of magnetization configurations for the array in Fig. 2(a), but here we only present the case with the largest static field. The static field, H_s, as a function of island thickness for the corner-to-corner separation between nearest neighbours from 1 nm to 141 nm is shown in Fig. 2(b). The largest static field of the central element produced by the neighbours is about 80 Oe for the 10 nm thick array and 240 Oe for the 30 nm thick array. The strength of the static field roughly decreases by a factor of 10 for the separation d between 1 nm and 141 nm. In addition, one sees from Fig. 2(a) that the dipolar stray field from the neighbours primarily affects the magnetization localised at the corners of the central island.

We now examine the SW excitations measured by BLS in the square ice-like geometry. BLS spectra of the thermal magnetic excitation were collected at room temperature in the backscattering geometry using a (3 + 3)-pass tandem

TABLE I. Comparison of the coercive fields, H_c, of the 10 nm and 30 nm thick elements between AFGM experiment and micromagnetic simulations.

Thickness (nm)	AFGM H_c (kOe)	Isolated-islands mean H_c (kOe)	4×4 units array H_c (kOe)
10	0.365 (±0.005)	0.537 (±0.066)	0.497 (±0.081)
30	0.553 (±0.005)	1.023 (±0.067)	0.806 (±0.076)

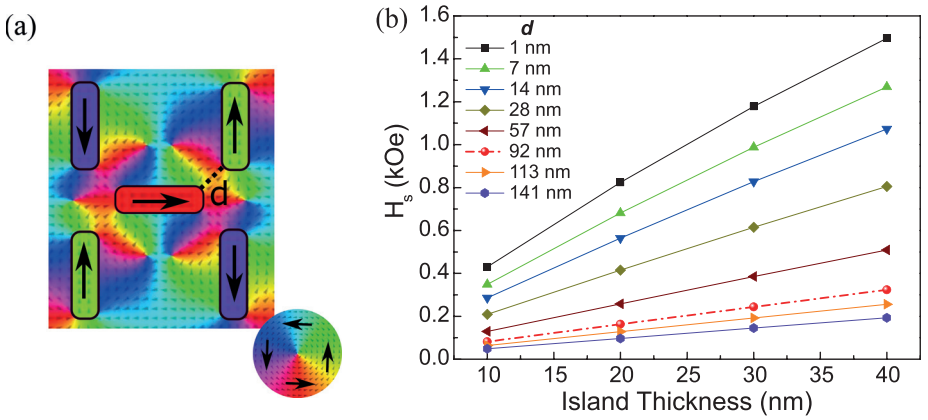

FIG. 2. (a) Distribution of the largest average stray field of the 30 nm thick ASI-like array where d is the corner-to-corner separation between the nearest islands, and the color code disk represents the orientations of magnetization in the element and the demagnetization out of the elements. (b) The largest static field H_s acting on the central element in (a) from the neighbouring elements as a function of island thickness for the corner-to-corner separation d from 1 nm to 141 nm.

Fabry-Perot interferometer. A monochromatic laser with a power of about 200 mW was focused at an incidence angle of 20° with respect to the sample normal. Since the light scattered from SWs has a polarization rotated by 90° with respect to the incident beam, an analyzer set at extinction suppresses the signal from both elastically scattered and surface phonon-scattered light. The laser spot has a diameter of about 30 μm so that several hundreds of ASI-like islands are illuminated at the same time and the achieved information therefore is averaged over a large number of the elements.[32] Dynamical coupling between the islands can be measured by the SW frequency dispersion (frequency vs. wave vector). This was studied in both the Damon-Eshbach and Backward Volume magnetostatic configurations when the applied field is horizontal (x-direction) with respect to the ASI-like principal axis.[22]

Examples of measured BLS spectra at the 4 kOe field are shown in Fig. 3. Well-defined, narrow BLS peaks were observed in the spectra obtained from the 10 nm thick ASI-like array (see Fig. 3(a)) with a clear frequency separation of larger than 3 GHz between two families of eigenmodes. Contrarily, peaks obtained in the spectra from 30 nm thick array (see Fig. 3(b)) are broad and more closely spaced in frequency.

Measured frequencies of the SWs are plotted as a function of the applied field for the 10 nm thick array, which was presented in the Li *et al*. paper,[22] and Fig. 4(a) for the 30 nm thick ASI-like array. The experimental data is shown by red square symbols. Above the coercive field, the dependence of the frequencies on field is linear. Below the coercive field, mode softening occurs as magnetizations of individual elements within the array reverse.

An analysis of the mode structure using micromagnetic simulation was performed as described elsewhere.[22] The independent elements are assumed to be infinitely separated so that no dynamic inter-island fields exist. The SW modes of a 2×2 units array with the 30 nm thick elements driven by field was also calculated (see Fig. S1(a) in the supplementary material), which reveals the influence of static field of neighbouring elements on the SW excitations. All SW resonances excited from this array with a 3 kOe field are overlapped with the superposition of SW resonances excited from isolated islands (I_h and I_v) with less than 0.35 GHz frequency discrepancy, as shown in Fig. S1(b) of the supplementary material. Therefore, using the independent-island model not only allows us to advantageously distinguish the contributions from the vertical and horizontal sublattices, but also is able to describe the SW behaviour of this square ASI-like array. In the simulation, the dimensionless damping parameter was set as 0.02, and a gyromagnetic ratio of $\gamma = 2.8$ GHz/kOe was determined from the separate FMR measurement and fitted by the Kittel

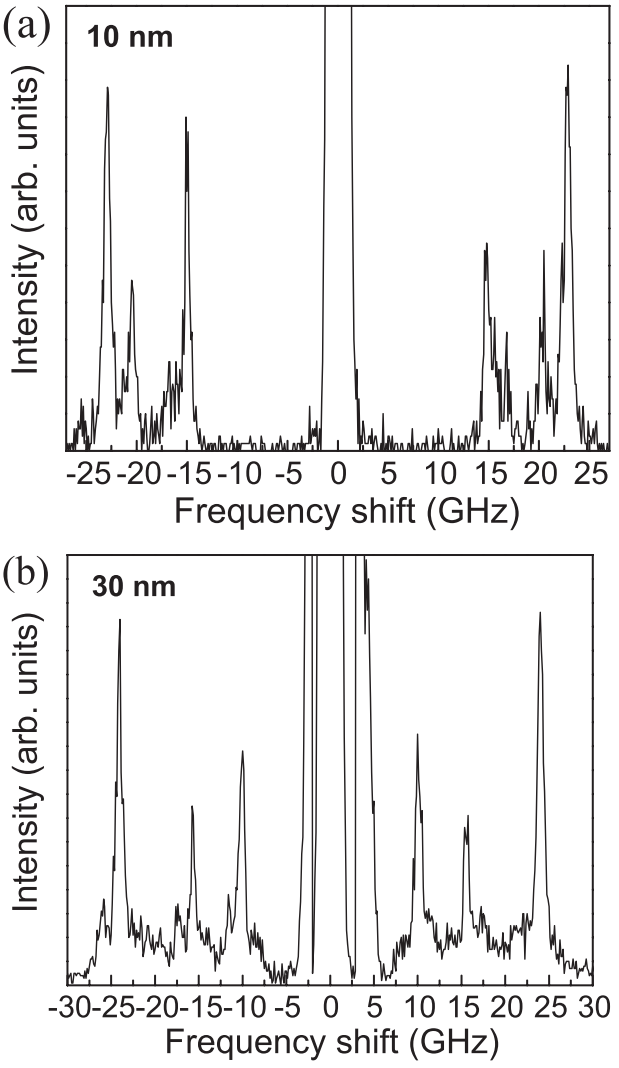

FIG. 3. BLS spectra of the (a) 10 nm and (b) 30 nm thick ASI-like arrays at the external field of 4 kOe. The incidence angle of the laser light upon the sample is 20°.

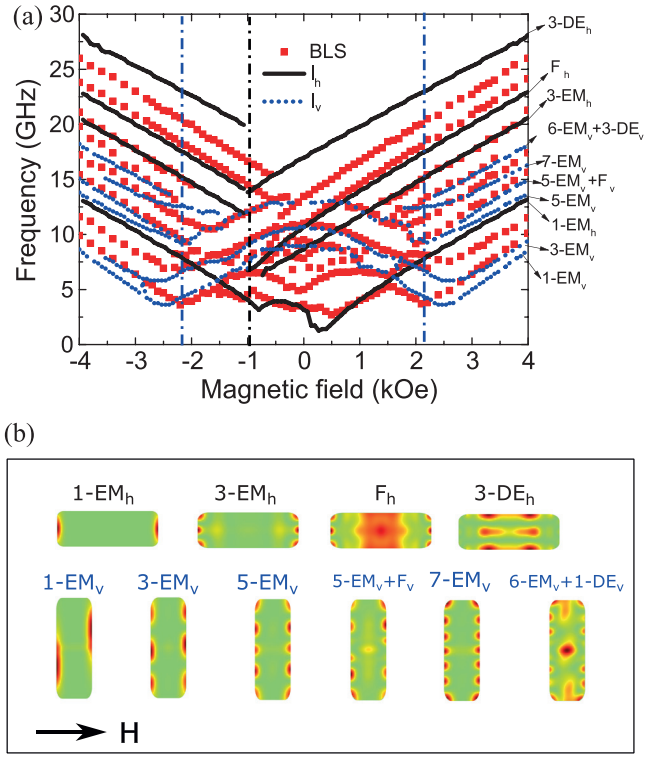

FIG. 4. (a) Frequencies of SW eigenmodes as a function of magnetic field *H*, applied along the *x*-direction for the 30 nm thick islands in square ASI-like array. Red squares are BLS experimental results; black solid and blue dotted lines indicate the simulation results for horizontally and vertically isolated islands with respect to the field, correspondingly. The blue and black dashed dotted lines indicate the switching fields of the horizontal and vertical islands, respectively. Labels indicate the spatial characters of the eigenmodes. (b) Spatial profiles of the out-of-plane m_z component of the dynamic magnetization in the 30 nm thick isolated element magnetized by the magnetic field *H* of 3 kOe.

function.[33] An external field is applied as in the hysteresis calculations, and varied from +4 kOe to −4 kOe. Qualitative agreement is obtained between experiment and simulations for both element thicknesses using the same magnetic parameters, but differing only in the element thickness. The 10 nm thick array shows a better agreement with the experimental values for frequency than the 30 nm thick array. As noted with regard to the hysteresis experiments and simulations, there is a static field produced on an element by neighbouring elements that has been neglected in the simulations. This leads to a coercivity that is too large because it does not take into account the different environments that elements at an array edge experience compared to those of the environment elements within the array. In addition, the element edge disorder is not included in the model. Kohli *et al*. show that this can also cause differences in the coercivity compared to simulated "ideal" islands.[34] In this regard, the evidence of stronger interaction coupling in the 30 nm thick sample may appear as a reduced coercivity. Also, the reduced coercivity field means that the minimal frequencies associated with softening at magnetic transitions will shift to lower fields and increase the frequency due to an increased internal field. From the simulation data of isolated elements shown in Fig. 4(a), we estimate this as a shift of field by an amount approximately equal to 0.5 kOe would increase the frequencies of the SWs in the linear regime by approximately 2 GHz.

Regarding the frequency evolution of magnetic eigenmodes as a function of the external magnetic field, we notice that, starting from +4 kOe and decreasing the field towards negative saturation, some of the eigenmodes are characterized by an almost linear behaviour (the black solid lines) with field while for some others there are frequency minima (the blue dotted lines). For fields between the minima frequency of these eigenmodes are characterized by a "bell" shape[35] and the minimal frequencies at low field are due to the reversal of the vertical element. The SW frequency, however, shows high field softening (the minima of the blue curves in Fig. 4(a)) and also low field softening (the minima in the black curves in Fig. 4(a)), which is, respectively, indicated by vertically blue and black dashed dotted lines. This means that we have access, through SW softening, to the separate reversal events of the field parallel (I_h) and field perpendicular (I_v) elements. In particular, by inspection of the simulated magnetization curves, one can assert that the frequency minima measured for the lowest frequency eigenmodes at ±2.1 kOe for the 30 nm thick array, are related to the saturation of the islands aligned perpendicular to the applied field while the other minima corresponds to reorientation of magnetization in islands aligned collinear to field *H*. By way of contrast, hysteresis measurements reflect the sum of two component orientations of sub-lattices with respect to the field, which is alone unable to distinguish between these separate reversals.

In Fig. 4(b), we show the calculated intensity profiles of the SW excitations of the independently horizontal and vertical islands, I_h and I_v. The eigenmodes are labelled according to the scheme proposed by Zivieri *et al*.[36] where "F" indicates a fundamental resonance localized in the central portion of the islands oriented horizontally (F_H) or vertically (F_V) with respect to the applied field direction H, "EM" indicates an edge mode, and "DE" designates the Damon-Eshbach mode with nodal planes parallel to the direction of the applied magnetic field.

EM eigenmodes are highly susceptible to surface and edge specific local anisotropy and exchange fields that can strongly affect the frequency of element excitations. Examples of these eigenmodes are shown in Fig.4(b). We note some of the discrepancies between the measured and calculated EM frequencies in Fig. 4(a), can be ascribed to the non-ideal shape of the elements, edge roughness, reduced edge magnetization, and surface anisotropy on the edge surface which lead to a smaller effective demagnetization field along the edges.[37]

It is interesting to notice that the F_h and F_V eigenmodes in the 30 nm thick island have a smaller spatial extension than the same mode in the 10 nm thick island that is displayed in the published paper.[22] This is connected to the spatial profile of the internal magnetic field. The internal magnetic field, H_{int}, defined as the sum of the Zeeman and static demagnetizing fields, due to magnetic free charges arising at the edges of the magnetic elements, has been calculated using the MuMax. For the thinner array, H_{int} is flatter in the central portion of the elements and more homogeneous (see Figs. 5(a) and 5(b)). We also notice that H_{int} for the 30 nm thick ASI-like array is always smaller than that of the

10 nm thick array, and this difference is responsible for the frequency shift of eigenmodes with the same spatial profile as observed in Fig. 4. Finally, the spatial extent of the EM mode (see Fig. 4(b)) when H is applied along the *x*-direction is larger than when H is parallel to the y-direction. This reflects the inhomogeneity region of H_{int} for the two magnetic field orientations with respect to the independent island.

III. DISCUSSION AND CONCLUSION

We now discuss the possibility of dynamic field interaction between islands of the ASI-like array by means of BLS detection and simulation. First, we have measured the SW dispersion for different field orientations, as described in Sec. II. A more detailed presentation of these results is in Ref. 22. No appreciable modification of the frequencies has been detected which suggests that these two arrays do not support a measurable magnon band width, and therefore collective SWs do not propagate. Instead the array behaves as a collection of elements which are affected only by the weak static field from the neighbours. This is consistent with the mode profiles calculated in Fig. 4(b). In a dense array of magnetic elements, the low frequency edge mode may couple between elements via a stray dynamic dipole field and the strength of the coupling would determine the width of the magnon band.[38] However, the fundamental mode is very much localised within an element, and the stray dynamic fields produced between elements are very small.

Here we pose a question of whether one can, in principle, design a square ice-like array that behaves as a magnonic crystal. Figure 6(a) displays the simulated SW frequencies of two elements of 30 nm thickness as a function of corner-to-corner distance between them. A 3 kOe applied field is parallel to the horizontal island. The frequencies of the two lowest-frequency modes (1-EM and 3-EM) will rise within the range of 1 GHz if *d* decreases to 1 nm. This change in frequency is due however to an increased static interelement coupling field, as shown in Fig. 2(b). In Fig. 6(b) the spatial profile of SW modes for 1 nm, 14 nm, and 92 nm island separation of Fig. 6(a) shows that there is no overlap between the two EM modes even when the islands nearly touch each other. Note that the F_v mode, which has a negligible overlap between islands, is independent of *d*.

In conclusion, we have measured the SWs on an array patterned into a square spin ice-like geometry and compared the frequencies obtained from 10 nm and 30 nm thick element which have a corner-to-corner separation between

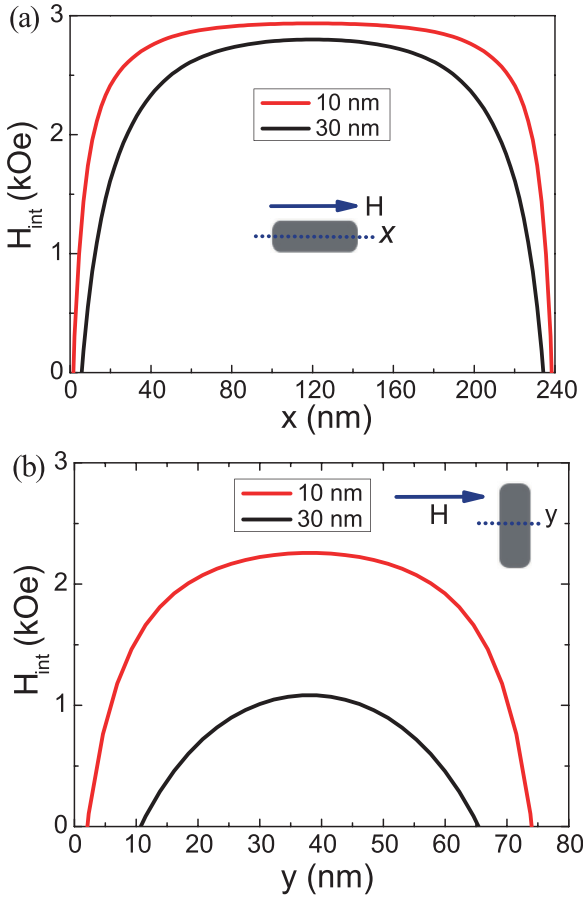

FIG. 5. Spatial profiles (a) x and (b) y of the internal field calculated along the central section of the element (the dotted line) for a magnetic field $H = 3.0$ kOe applied along the arrow direction.

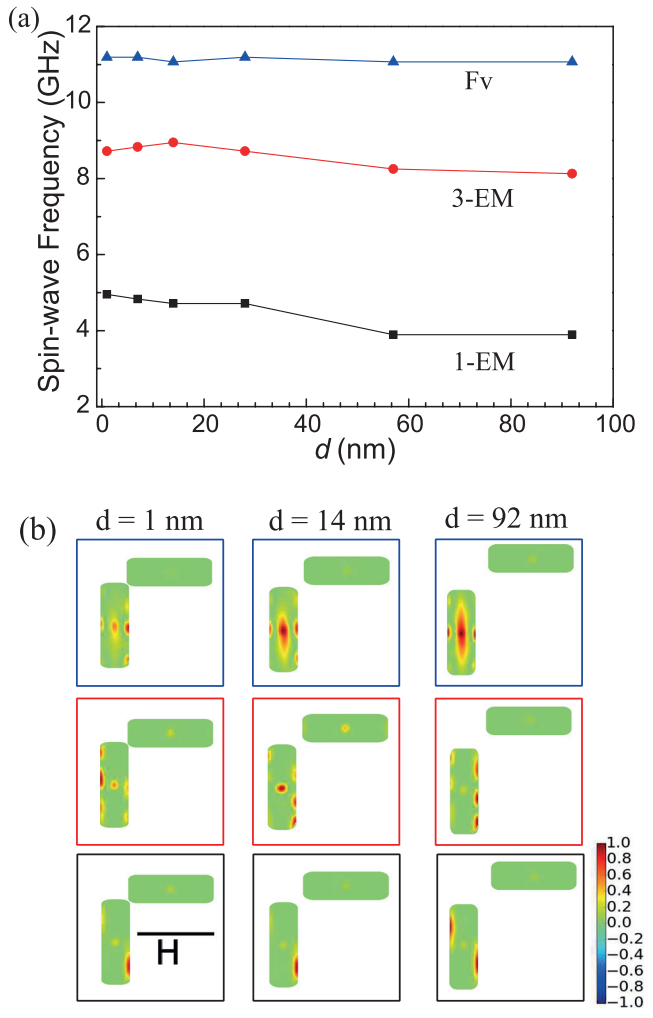

FIG. 6. (a) Frequencies of SW modes of 30 nm thick two-element array as a function of corner-to-corner separation *d* between the nearest neighbours. (b) Spatial profiles of the out-plane m_z component of the two elements with 1 nm, 14 nm, and 92 nm separation. Note that the line is a guide to the eyes, and the *d* is not scaled in the profile map.

nearest island of 92 nm. Softening observed in the edge mode spectra as a function of applied magnetic field can be identified with reversal of different orientations of magnetic islands. This allows us to use SW spectra to differentiate reversals of elements with axes parallel to the applied magnetic field from elements with axes perpendicular to the applied field.

We do find some evidence for observable static field interactions between 30 nm thick elements. This evidence is determined by the coercive fields of experiment and simulated array which are substantially less than those expected of isolated elements. Inter-element interactions may reduce the array coercivity by assisting the reversal of elements at the array edges and corner through cooperative effects that can lead to reduced coercivity of the entire array. This interaction may also contribute weakly to the SW frequencies.

Lastly, we note that most of the SW excitations observed in two ASI-like arrays of 10 nm and 30 nm thickness belong to the class of edge localized eigenmodes. This means that their measurement provides, at least in principle, information about surface effects that determine the frequency of SW eigenmodes confined to individual elements.

SUPPLEMENTARY MATERIAL

See supplementary material for the frequencies of simulated SW modes in a 2×2 units (12 elements) array as a function of the external field and the comparison of the SW modes with the 3 kOe field among the 2×2 units array, horizontally and vertically isolated islands.

ACKNOWLEDGMENTS

Financial support for this work was provided by EPSRC (Grant Nos.: EP/L002922/1 and EP/L00285X/1). We gratefully acknowledge that the results of micromagnetic simulation here made use of the Emerald High Performance Computing Facility. The data underpinning this paper are available at http://dx.doi.org/10.5525/gla.researchdata.391.

[1]L. J. Heyderman and R. L. Stamps, J. Phys.: Condens. Matter **25**, 363201 (2013).
[2]R. F. Wang, C. Nisoli, R. S. Freitas, J. Li, W. McConville, B. J. Cooley, M. S. Lund, N. Samarth, C. Leighton, V. H. Crespi, and P. Schiffer, Nature **439**, 303 (2006).
[3]J. P. Morgan, A. Stein, S. Langridge, and C. H. Marrows, Nat. Phys. **7**, 75 (2011).
[4]C. Nisoli, R. Wang, J. Li, W. F. McConville, P. E. Lammert, P. Schiffer, and V. H. Crespi, Phys. Rev. Lett. **98**, 217203 (2007).
[5]Z. Budrikis, P. Politi, and R. L. Stamps, Phys. Rev. Lett. **105**, 089901 (2010).
[6]E. Mengotti, L. J. Heyderman, A. Fraile Rodríguez, A. Bisig, L. Le Guyader, F. Nolting, and H. B. Braun, Phys. Rev. B **78**, 144402 (2008).
[7]Y. L. Wang, Z. L. Xiao, A. Snezhko, J. Xu, L. E. Ocola, R. Divan, J. E. Pearson, G. W. Crabtree, and W. K. Kwok, Science **352**, 962 (2016).
[8]A. Farhan, P. M. Derlet, A. Kleibert, A. Balan, R. V. Chopdekar, M. Wyss, J. Perron, A. Scholl, F. Nolting, and L. J. Heyderman, Phys. Rev. Lett. **111**, 057204 (2013).
[9]Y. Perrin, B. Canals, and N. Rougemaille, Nature **540**, 410–413 (2017).
[10]G. Gubbiotti, M. Conti, G. Carlotti, P. Candeloro, E. Di Fabrizio, K. Y. Guslienko, A. Andre, C. Bayer, and A. N. Slavin, J. Phys.: Condens. Matter **16**, 7709 (2004).
[11]C. Bayer, J. Jorzick, B. Hillebrands, S. O. Demokritov, R. Kouba, R. Bozinoski, A. N. Slavin, K. Y. Guslienko, D. V. Berkov, N. L. Gorn, and M. P. Kostylev, Phys. Rev. B **72**, 064427 (2005).
[12]M. Dvornik, P. V. Bondarenko, B. A. Ivanov, and V. V. Kruglyak, J. Appl. Phys. **109**, 07B912 (2011).
[13]P. S. Keatley, P. Gangmei, M. Dvornik, R. J. Hicken, J. Grollier, and C. Ulysse, Phys. Rev. Lett. **110**, 187202 (2013).
[14]V. S. Bhat, J. Sklenar, B. Farmer, J. Woods, J. T. Hastings, S. J. Lee, J. B. Ketterson, and L. E. De Long, Phys. Rev. Lett. **111**, 077201 (2013).
[15]V. S. Bhat, J. Sklenar, B. Farmer, J. Woods, J. B. Ketterson, J. T. Hastings, and L. E. De Long, J. Appl. Phys. **115**, 17C502 (2014).
[16]J. Sklenar, V. S. Bhat, L. E. Delong, and J. B. Ketterson, J. Appl. Phys. **113**, 17B530 (2013).
[17]M. B. Jungfleisch, W. Zhang, E. Iacocca, J. Sklenar, J. Ding, W. Jiang, S. Zhang, J. E. Pearson, V. Novosad, J. B. Ketterson, O. Heinonen, and A. Hoffmann, Phys. Rev. B **93**, 100401(R) (2016).
[18]S. Gliga, A. Kákay, R. Hertel, and O. G. Heinonen, Phys. Rev. Lett. **110**, 117205 (2013).
[19]X. Zhou, G. L. Chua, N. Singh, and A. O. Adeyeye, Adv. Funct. Mater. **26**, 1437 (2016).
[20]I. R. B. Ribeiro, J. F. Felix, L. C. Figueiredo, P. C. Morais, S. O. Ferreira, W. A. Moura-Melo, A. R. Pereira, A. Quindeau, and C. I. L. de Araujo, J. Phys.: Condens. Matter **28**, 456002 (2016).
[21]Y. Yahagi, C. R. Berk, B. D. Harteneck, S. D. Cabrini, and H. Schmidt, Appl. Phys. Lett. **104**, 162406 (2014).
[22]Y. Li, G. Gubbiotti, F. Casoli, F. Trindade, S. A. Morley, M. C. Rosamond, E. Linfield, H. Marrows, S. Mcvitie, and R. L. Stamps, J. Phys. D: Appl. Phys. **50**, 015003 (2017).
[23]G. Gubbiotti, L. Albini, G. Carlotti, M. De Crescenzi, E. Di Fabrizio, A. Gerardino, O. Donzelli, F. Nizzoli, H. Koo, and R. D. Gomez, J. Appl. Phys. **87**, 5633 (2000).
[24]E. Iacocca, S. Gliga, R. L. Stamps, and O. Heinonen, Phys. Rev. B **93**, 134420 (2016).
[25]F. Montoncello, L. Giovannini, F. Nizzoli, P. Vavassori, M. Grimsditch, T. Ono, G. Gubbiotti, S. Tacchi, and G. Carlotti, Phys. Rev. B **76**, 024426 (2007).
[26]F. Montoncello, L. Giovannini, F. Nizzoli, H. Tanigawa, T. Ono, G. Gubbiotti, M. Madami, S. Tacchi, and G. Carlotti, Phys. Rev. B **78**, 104421 (2008).
[27]A. Vansteenkiste, J. Leliaert, M. Dvornik, M. Helsen, F. Garcia-Sanchez, and B. Van Waeyenberge, AIP Adv. **4**, 107133 (2014).
[28]N. Smith, D. Markham, and D. Latourette, J. Appl. Phys. **65**, 4362 (1989).
[29]J. Ben Youssef, N. Vukadinovic, D. Billet, and M. Labrune, Phys. Rev. B **69**, 174402 (2004).
[30]Z. Budrikis, J. P. Morgan, J. Akerman, A. Stein, P. Politi, S. Langridge, C. H. Marrows, and R. L. Stamps, Phys. Rev. Lett. **109**, 037203 (2012).
[31]R. V. Hügli, G. Duff, B. O'Conchuir, E. Mengotti, A. F. Rodríguez, F. Nolting, L. J. Heyderman, and H. B. Braun, Philos. Trans. R. Soc., A **370**, 5767 (2012).
[32]G. Carlotti and G. Gubbiotti, Riv. Nuovo Cimento **22**, 1 (1999).
[33]C. Kittel, Phys. Rev. **73**, 155 (1948).
[34]K. Kohli, A. Balk, J. Li, S. Zhang, I. Gilbert, P. Lammert, V. Crespi, P. Schiffer, and N. Samarth, Phys. Rev. B **84**, 180412 (2011).
[35]V. Flovik, F. Macià, J. M. Hernàandez, R. Bručas, M. Hanson, and E. Wahlström, Phys. Rev. B **92**, 104406 (2015).
[36]R. Zivieri, F. Montoncello, L. Giovannini, F. Nizzoli, S. Tacchi, M. Madami, G. Gubbiotti, G. Carlotti, and A. O. Adeyeye, Phys. Rev. B **83**, 054431 (2011).
[37]R. D. McMichael and B. B. Maranville, Phys. Rev. B **74**, 024424 (2006).
[38]S. Tacchi, M. Madami, G. Gubbiotti, G. Carlotti, H. Tanigawa, T. Ono, and M. P. Kostylev, Phys. Rev. B: Condens. Matter Mater. Phys. **82**, 024401 (2010).